


ORIGINAL ARTICLE

Secretome from prolonged high-density human Wharton's jelly stem cell culture accelerates wound healing in both in vitro and in vivo models

Jiah Shin Chin¹ | Mandy Li Ling Tan¹ | Priscilla Lay Keng Lim² |
Bhavya Sharma³ | Aimin Yeo⁴ | Yi Bing Aw⁴ | Yi Zhen Ng² |
Carine Bonnard^{2,3} | David L. Becker^{1,3,5} | Pamela Mok⁴ 

¹Lee Kong Chian School of Medicine, Nanyang Technological University, Singapore, Singapore

²A*STAR Skin Research Labs, Agency for Science, Technology and Research, Singapore, Singapore

³Skin Research Institute of Singapore, Singapore, Singapore

⁴Celligenics Pte Ltd, Singapore, Singapore

⁵National Skin Centre, Singapore, Singapore

Correspondence

Pamela Mok, Celligenics Pte Ltd,
30 Biopolis Street, #B2-15E, Singapore
138671, Singapore.
Email: pamela@celligenics.com

Funding information

Singapore innovation grant, Grant/Award
Number: SIG2005; Celligenics pte ltd

Abstract

The complex of biofactors secreted by mesenchymal stem cells, termed the secretome, can promote wound healing. Studies using this secretome often utilise material collected from short term and sub-confluent lab-scale cultures. Secretome was derived from prolonged culture of high-density industrial scale human Wharton's jelly stem cells and its effects on wound healing was assessed. In vitro cell proliferation and scratch closure assays showed that secretome treatment dose-dependently increased cell proliferation and promoted scratch closure. Subsequently, using biopsy punch, circular wounds were created on three-dimensional de-epidermised dermis human skin equivalent (in vitro) where secretome-treated wounds showed accelerated wound closure, and enhanced epithelial proliferation and differentiation were observed and quantified. In an in vivo rat acute wound model, secretome applied to the back of test animals greatly enhanced wound healing by promoting re-epithelialisation, vascularisation and granulation maturation. In conclusion, secretome derived from prolonged culture of high-density industrial scale two-dimensional human Wharton's jelly stem cells possesses potent wound healing properties. This could greatly lower the cost of production and facilitate development of highly efficacious secretome-based wound healing products.

This work was performed at A*STAR Skin Research Institute Singapore; Clinical Sciences Building, Lee Kong Chian School of Medicine, Singapore; and Celligenics Pte Ltd, Singapore.

This is an open access article under the terms of the [Creative Commons Attribution-NonCommercial-NoDerivs](https://creativecommons.org/licenses/by-nc-nd/4.0/) License, which permits use and distribution in any medium, provided the original work is properly cited, the use is non-commercial and no modifications or adaptations are made.

© 2025 Celligenics Pte Ltd and The Author(s). *International Wound Journal* published by Medicalhelplines.com Inc and John Wiley & Sons Ltd.

KEYWORDS

in vitro 3D skin, mesenchymal stem cells, secretome, Wharton jelly, wound healing

Key messages

- Highly cost-efficient secretome derived from prolonged culture of high-density industrial scale two-dimensional human Wharton's jelly stem cells strongly enhances wound healing.
- In vitro cell proliferation and scratch assays, three-dimensional skin models, and rat acute wound models were used to assess the wound healing potential of human Wharton's jelly stem cell secretome.
- This study showed that human Wharton's jelly stem cell secretome accelerated wound healing by promoting re-epithelialisation, re-vascularisation, wound bed maturation, and inflammation resolution.

1 | INTRODUCTION

Cutaneous wound healing after injury normally progresses through four regulated stages – haemostasis, inflammation, cell proliferation, and maturation (remodelling).^{1,2} This process is disrupted in chronic wounds, which are still open after 4–12 weeks, and their treatment and management poses a tremendous economic burden.^{3,4} In the USA alone, this represents over \$28B USD per year.⁵

Due to the advancement of cell related technologies in recent years, mesenchymal stem cells (MSCs) have emerged as a potential therapy for wound healing.^{6–9} MSCs, shown to aid in wound healing, include those derived from adult tissue such as bone marrow,¹⁰ adipose tissue,⁶ neonatal tissue such as placenta¹¹ and umbilical cord.⁹ However, despite their promise, there are some disadvantages^{12,13} to the use of MSCs in wound treatment because they typically need to be seeded on a scaffold or embedded in a matrix or gel prior to application.^{14,15} This is time-consuming and the use of living cells precludes a ready-made, off-the shelf product. Handling, transportation and storage of products incorporating living cells also requires stringent conditions and trained personnel to maintain cell viability, product function and to prevent contamination. Such treatment modalities are difficult to upscale, costly and can only be performed at hospitals and/or clinics with adequate facilities and trained staff. These technical, logistical and economic challenges hinder the use of stem cells in wound therapy.

Research has shown that many of the beneficial effects of MSCs, such as immunomodulatory effects, are mediated by paracrine (secreted) factors (e.g. growth factors, cytokines, exosomes) secreted by these cells.^{16,17} An attractive alternative to the direct use of MSCs are products containing their paracrine factors instead, which may include the whole secretome or a subset such as the

exosomes. The use of such cell-free material would confer many advantages over the cells, including greater scalability, accessibility, and easier logistics. There is clear evidence in the literature showing an acceleration in the healing of chronic wounds, such as diabetic ulcers, after treatment with MSC-derived secretome^{18,19} or exosomes.²⁰

While the use of MSC secreted factors is highly desirable, there are still challenges to overcome in the clinical application of such cell free material, one of which is the relatively high cost of production particularly for exosomes.²¹ Of note, studies on the therapeutic effects of mesenchymal stem cell paracrine factors often utilise material obtained from a single collection of culture medium produced by short term (e.g. 1–3 days) subconfluent cultures,^{22–24} which can translate to a much higher cost of production. This cost could be substantially reduced if a greater quantity of secreted factors could be collected from a single culture and over a longer period. This would pave the way for development of a more commercially viable therapeutic product.

This study describes a secretome derived from prolonged culture of high-density industrial scale two-dimensional (2D) human Wharton's jelly stem cells (hWJSCs). Here, the authors assessed the wound healing effects of the secretome in vitro using 2D assays and a 3D skin model and in vivo using rats.

2 | METHODS

2.1 | Human WJSC isolation, culture and cryopreservation

Human Wharton's jelly stem cells were isolated from umbilical cords obtained from healthy neonates after at least 36 weeks gestation. Prior to umbilical cord

collection, informed consent was obtained from the parents by Celligenics Pte Ltd, a registered tissue bank in Singapore. Umbilical cords were washed in Hanks balanced salt solution (HBSS) to remove blood. Umbilical cords were then cut into pieces and each piece was subsequently cut open lengthwise. The Wharton's jelly was then carefully excised from each piece and cut into small pieces which were then transferred into a tissue culture dish containing sufficient Celligenics hWJSC culture medium to cover the bottom of the dish. The explanted tissue was incubated in a 37°C incubator with 5% carbon dioxide. Culture medium (proprietary formulation) was changed every 2–3 days while cells migrated out from the tissue. When there was substantial outgrowth from the explants, they were removed and the cells were dissociated from the dish by incubating with TrypLE™ for 10 min at 37°C in a carbon dioxide (CO₂) incubator after washing with HBSS. After TrypLE™ incubation, the TrypLE™ was diluted with culture medium, and the dissociated cells were collected into a centrifuge tube. Collected cells were centrifuged at 300 g for 5 min and resuspended in culture medium for counting after removing the supernatant. Cells were counted using Trypan Blue staining (according to manufacturer's instructions), cryopreserved in CryoStor10 and placed in liquid nitrogen for long term storage.

2.2 | Human WJSC characterisation

Cryopreserved hWJSCs were removed from liquid nitrogen storage and rapidly thawed in a 37°C water bath. Thawed cells were diluted with culture medium, centrifuged at 300 g for 5 min, and resuspended in culture medium for viability measurement counting using Trypan Blue staining after removing the supernatant. hWJSCs were seeded in 6-well culture plates in duplicate wells and culture medium was changed every 2–3 days. Cells were subcultured and counted every 4–5 days. For trilineage differentiation assay to confirm stem cell lineage, hWJSCs at passage 4 were seeded in 24-well culture plates and differentiated using StemPro™ chondrogenesis/osteogenesis differentiation kit (Gibco, USA) and MesenCult™ adipogenic differentiation kit (Stem Cell Technologies, Canada) according to manufacturers' instructions. After 18–21 days of differentiation, cells were stained with Alizarin Red for osteogenesis, Oil Red O for adipogenesis, Alcian Blue for chondrogenesis and imaged under bright field using an Olympus IX71 inverted microscope (Olympus, Japan) at 4× objective.

For cell surface marker expression, hWJSCs at passage 3 were dissociated using TrypLE™ by incubating the cells with TrypLE™ for 5 min at 37°C in a CO₂

incubator after washing with HBSS. The dissociated cells were collected, centrifuged at 300 g for 5 min, and fixed in 2% paraformaldehyde (1 million cells per 100 µL) at 4°C for 15 min. After fixation, hWJSCs were washed twice by adding FACS buffer (2% FBS in PBS) to the cells, centrifuging the cell suspension at 300 g for 5 min and removing the supernatant after each wash. Thereafter, hWJSCs were incubated with antibodies to human CD34, CD73, CD166 (APC-conjugated), CD14, CD45, CD90, CD105 (FITC-conjugated) at 4°C for 15 min. Unbound antibody was removed by repeating the above wash step 3 times. The stained hWJSCs were resuspended in FACS buffer and data was acquired with FACSCelesta™ Cell Analyser (Becton Dickinson, USA) and analysed using FACSdiva v8.0.2 (Becton Dickinson, USA).

2.3 | Secretome production

Secretome from human WJSCs was produced according to methods described in patent application WO2023/101603A1. Briefly, cryopreserved hWJSCs were recovered and cultured for one passage and subsequently seeded in Corning® HYPERFlasks® (Corning, USA). At 95%–100% confluency, culture medium was removed and hWJSCs were washed twice with HBSS. Cells were then incubated in serum-free medium. Secretome was periodically collected and replaced with fresh medium every 2–3 days. The secretome collected was concentrated 50-fold via ultrafiltration and stored at –80°C. Concentrated secretome from three batches was pooled prior to analysis and testing in in vitro and in vivo wound studies.

2.4 | Secretome characterisation

Total secretome protein content was quantified by Coomassie Blue Plus Protein Assay reagent (Bio-Rad, USA). Briefly, 50 µL of sample was loaded into a clear 96-well microplate in duplicate and 250 µL of Coomassie Blue Plus Protein Assay reagent was added to the samples and then incubated for 10 min at room temperature. After incubation, absorbance at 560 nm was read using a VICTOR3™ Multilabel Plate Reader (Perkin Elmer, USA). Absorbance values were compared to a standard curve to quantify protein content.

Secretome factors were quantified by multiplex using the 48-Plex Bio-Plex Pro human cytokine screening panel according to manufacturer's instructions. Sample-antibody-bead complexes were re-suspended in sheath fluid for acquisition on the FLEXMAP® 3D (Luminex) using xPONENT® 4.0 (Luminex) software. Data analysis was done on Bio-Plex Manager™ 6.1.1 (Bio-Rad).

Standard curves were generated with a 5-PL (5-parameter logistic) algorithm, reporting values for both mean fluorescence intensity (MFI) and concentration data.

Secretome extracellular vesicle content in the pooled concentrated secretome was directly quantified using a commercial ELISA kit (PS Capture™ Exosome ELISA Kit, FUJIFILM Wako Chemicals, Japan) according to manufacturer's instructions and absorbance at 450 nm was read using the plate reader indicated above. Absorbance values were compared to a standard curve to quantify extracellular vesicle content.

2.5 | Cell proliferation assay

Cell proliferation ($n = 10$ – 12 over 3 repeats) was assessed in 96-well tissue culture plates using non-immortalised human adult dermal fibroblasts (HDF) and HaCaT keratinocytes. Cells were seeded in minimal serum culture medium (DMEM with 0.2% Foetal Bovine Serum (FBS), 1X GlutaMAX, 1X Non-Essential Amino Acid (NEAA), 1X penicillin–streptomycin) with and without secretome. Cells were then incubated for 3 days at 37°C in a CO₂ incubator. After incubation, the cells were washed with HBSS before fixing in 1.5% PFA for 30 min at room temperature. After fixation, cells were stained with 0.5% crystal violet solution for 10 min at room temperature. The crystal violet was removed, and the cells washed with water until the solution was clear. Cells were air-dried, imaged on bright field using an Olympus IX71 inverted microscope (Olympus, Japan) at 4x objective and 1 N acetic acid solution was added to the cells to solubilise the crystal violet. After solubilisation, the absorbance was read at 560 nm using a spectrophotometer (Perkin Elmer, USA) and cells in each well were quantified by comparing the absorbance with the absorbance of a cell standard which was stained and solubilised using the same method. The number of cells was expressed as a percentage relative to the cells that were incubated without secretome.

2.6 | Scratch assay

Scratch assays ($n = 10$ – 12 over 3 repeats) were carried out in 96-well tissue culture plates using non-immortalised human adult dermal fibroblasts (HDF) and HaCaT keratinocytes. Cells were seeded in culture medium (DMEM with 10% Foetal Bovine Serum (FBS), 1X GlutaMAX, 1X Non-Essential Amino Acid (NEAA), 1X penicillin–streptomycin) and grown to confluence. At confluence, cells were scratched using an in-house developed scratch assay device.²⁵ After scratching, the cells

were washed with HBSS, imaged, and then incubated at 37°C in a CO₂ incubator for 2 (HaCaT) or 3 (HDF) days in minimal serum culture medium with media control or with secretome. Scratched cells were imaged on Phase Contrast at 4x objective using the imaging template with an Olympus IX71 inverted microscope (Olympus, Japan). After incubation, cells were washed with HBSS and fixed in 1.5% paraformaldehyde (PFA) for 30 min at room temperature. After fixation, cells were stained with 0.025% safranin O and imaged on bright field an Olympus IX71 inverted microscope (Olympus, Japan) at 4x objective using the imaging template. Scratch area (area without cells) pre- and post-treatment was traced and quantified using FIJI Software.²⁶ The percentage wound closure was calculated by dividing the scratch area after treatment by the scratch area before treatment and multiplying this value by 100.

2.7 | Skin supply & human epidermal keratinocyte culture

Approval was obtained from the A*STAR Human Biomedical Research Office, under the IRB 2019–094 for the use of ethically sourced human skin materials from Unison Collaborative (Singapore) and CellResearch Corporation (Singapore). Written informed consent was obtained from patients undergoing abdominoplasties before skin collection and all patient identifiers were removed. The study was conducted with strict adherence to the Human Biomedical Research Act 2015 of Singapore.

Early passage of de-identified primary human keratinocytes was obtained from the Asian Skin Biobank at the Skin Research Institute of Singapore (SRIS). The keratinocytes were derived from abdominal skin tissues of a 38-years-old Chinese female donor. Frozen cells were thawed and cultured on a layer of gamma-irradiated 3 T3 feeder cells in Full Green's medium (FG) at 37°C with 5% CO₂ and 95% humidified ambient air.

2.8 | Preparation of de-epidermized dermis-human skin equivalent (DED-HSE) wound model

The DED-HSEs were prepared from full-thickness abdomen skin tissues donated by two independent female donors using a method previously described with some adjustments and modifications.²⁷ Briefly, fresh human skin tissues were treated with 1 M NaCl at 37°C overnight. Epidermis was peeled off and 1.5 cm × 1.5 cm of De-Epidermized Dermis (DED) were cut and placed with papillary side faced up in a 24-well plate. Stainless-steel

rings (Aix-Scientifics, Aachen, Germany) were carefully aligned and centred onto each DED, and 2×10^4 human keratinocytes were seeded in each ring. After 2 days in culture, the rings were removed and the DEDs were transferred on sterile stainless-steel chairs placed in 6-well plate with FG medium. DEDs were kept in air-liquid interface for 9–11 days to facilitate full epidermal growth and stratification. After 9–11 days in culture, 4 mm partial-thickness wounds were created in each DED-HSE, with a biopsy punch (Stiefel, Castle Hill, NSW, Australia) excising through the epidermis. Four conditions were tested in triplicates, including media control (control medium without secretome factors), secretome, blank (untreated, negative control) and 100% FBS (Fetal Bovine Serum, positive control).

2.9 | Measurement of DED-HSE wound closure and toxicity via MTT assay

At 0, 4, and 7 days post-wounding, DED-HSEs from each treatment group ($n = 6$ from 2 donors) were harvested and placed in a 50 mm-petri dish containing 0.5 mg/mL of 3-(4,5-Dimethylthiazol-2-yl)-2,5-Diphenyltetrazolium Bromide (MTT) solution. The samples were incubated in 5% CO₂ at 37°C for 90 min to allow the formation of formazan. Viable cells with active metabolism react with the tetrazolium ring of the MTT producing a purple-coloured insoluble formazan product. Images of the DEDs were captured using Nikon SMZ745T Stereo Dissecting microscope to observe cell viability across the wounded tissue and to measure wound closure. Using Image J software (<https://imagej.nih.gov/ij/>), the area with no closure (X) was measured and subtracted from the original wound area at day 0 (Y) to obtain the re-epithelialized area (percent healed area).

2.10 | Full-thickness excisional wounding in rats

Male Sprague–Dawley rats were purchased from InVivos and housed in the Animal Research Facility of the Lee Kong Chian School of Medicine, Singapore. Animals were 9–10 weeks of age and had an average weight of 350–400 g prior to the start of the experiment. All animal procedures were performed in accordance with the approved animal protocols obtained from the Institutional Animal Care and Use Committee (IACUC) of Nanyang Technological University (IACUC Project Number A19055). Rats ($n = 3$) were anaesthetised with 4% iso-flurane and maintained at 2% for the duration of the experiment. Subsequently, the dorsal skin of the rats was

shaved with an electric hair trimmer, with care not to induce trauma with razor teeth. Depilatory cream (Nair®) was applied to the shaved skin and left for 2 min. Thereafter, the cream and remaining hair was removed with warm wet gauze. Clean dry gauze was then used to wipe off all remaining hair removal cream to ensure there was no risk of skin lesions and that the prepared skin was completely bare. The shaved back was wiped with 70% ethanol and the skin was tented away from the dorsum to generate 6 full-thickness excisional wounds using a 6 mm biopsy punch (#12–460–412, Integra Miltex, USA). Wounds were left untreated, treated with Pluronic gel with control medium, or treated with Pluronic gel with secretome on 0, 1 and 2 days post-wounding. Buprenorphine at concentrations of 0.1 mg/kg was delivered subcutaneously after wounding and the rats were housed individually and monitored for their health and weight status daily until the day of harvest.

2.11 | Optimisation of secretome carrier for rat acute wound model study

Pluronic gel was selected as the carrier for the secretome in our acute rat wound study due to its thermo-reversible properties, which allows it to transition from a liquid state below 8°C—facilitating easy mixing with the secretome—to a solid state at physiological temperature (37°C), ensuring retention within the wound. Gels were prepared at four concentrations (15%, 20%, 25%, and 30% w/v), each dissolved in either distilled water or in solutions containing 300 µg/mL of secretome control or secretome, with 1% crystal violet added for visualisation. 30 µL of each gel formulation was pipetted into wells on a 12-well plate and allowed to solidify on a heat plate set to 37°C. For each gel type, five replicates were prepared. Following solidification, 500 µL of pre-warmed 1X PBS was added to each well, refreshed every 5 min, while degradation was monitored by imaging every 5 min using a Leica MZ FLIII fluorescence stereomicroscope, to determine the optimal gel concentration for effective secretome delivery and retention at the wound site.

2.12 | Wound harvesting and histological processing

Rats were euthanized by carbon dioxide (CO₂) inhalation and wounds harvested at 3 and 5 days post-wounding. On the day of the harvest, 1 cm² of wounded skin tissue was harvested and bisected before fixation in 4% paraformaldehyde overnight. Half of the fixed tissue was used for paraffin-embedding. Prior to being transferred to a

tissue processor (Leica Biosystems, HistoCore PEARL, Germany), wounds were placed in cassettes and immersed in 70% ethanol (Aik Moh Paints and Chemicals, Singapore) overnight at 4°C. Finally, tissues were embedded in wax and sectioned at 5 µm using a microtome (Leica Biosystems, RM2245, Germany).

2.13 | Haematoxylin and eosin (H&E) staining

For DED-HSE samples, after MTT assay, each DED-HSE was bisected into two equal halves where re-epithelialization looked the most advanced. The tissues were fixed in 10% neutral buffered formalin and processed into formalin-fixed paraffin embedded (FFPE) blocks. They were subsequently sectioned and stained with H&E according to standard histological protocols. Full sections were scanned using Zeiss Axio Scan.Z1 system (Carl-Zeiss, Oberkochen, Germany). Wound edge images were taken with Olympus System Microscope BX43 (Olympus LS, Tokyo, Japan), at objective 20X or zoomed in from the scanned images.

For rat tissue samples, histological sections (5 µm) were stained with H&E using an autostainer (Leica Biosystems, ST5010 Autostainer XL, Germany). Tissue sections were dewaxed in clearene (#3803600E, Leica Biosystems, Germany) and rehydrated through a graded series of ethanol (Aik Moh Paints and Chemicals, Singapore) to water (2 × clearene for 5 min, 2 × 100% ethanol for 2 min, 2 × 95% ethanol for 2 min and 1 × 70% ethanol for 2 min). Subsequently, slides were immersed in haematoxylin (#3801570, Leica Biosystems, Germany) stain for 1 min followed by an immediate rinse in running tap water to remove excess haematoxylin stain. To remove background staining, slides were then submerged in 0.3% acetic acid [0.3% (v/v) concentrated hydrochloric acid, 70% (v/v) ethanol and 29.97% (v/v) distilled water (DI)] and rinsed in running tap water. Thereafter, the slides were quickly dipped into Scott's tap water [0.5% (v/v) sodium bicarbonate and 5% (v/v) magnesium sulphate in DI water] to enhance the contrast of the H&E stain and rinsed with running tap water. Slides were then immersed into alcoholic eosin Y 515 stain (#3801615, Leica Biosystems, Germany) for 2 min. Subsequently, the slides underwent a dehydration process through a series of ethanol and then clearene (1 × 70% ethanol for 2 min, 2 × 95% ethanol for 2 min, 2 × 100% ethanol for 2 min and 1 × clearene for 2 min). Slides were then mounted and sealed with a coverslip using Limonene mounting medium. When dry, the slides were imaged on a slide scanner (Zeiss Axioscan). All H&E staining was carried out with an autostainer (Leica Biosystems, ST5010

Autostainer XL, Germany) and imaged using a slide scanner (20× objective, Carl Zeiss, Zeiss Axioscan Z1, Germany). Tissues were analysed and regions of interest captured using Zeiss Zen Black software (Carl Zeiss, Germany).

2.14 | Immunohistochemistry (IHC) staining

For DED-HSE samples, FFPE blocks were sectioned and processed for IHC using standard protocols.²⁸ Three markers, Tumour protein 63 (p63), Keratin 14 (K14) and Keratin 10 (K10) were selected to assess the effects of treatment on cell proliferation and differentiation. The following primary antibodies (dilution) were used: mouse monoclonal anti-K10 (1:200), mouse monoclonal anti-K14 (1:25), and mouse monoclonal anti-p63 (1:50). Heat-induced epitope retrieval of the FFPE sections used 90°C heated 0.01 M sodium citrate buffer pH 6 for 15 min.^{29,30}

2.15 | Measurement of re-epithelialization in rat wound tissue sections

Regions of interest (ROIs) (2000 µm by 2000 µm) in the wound edges of H&E-stained sections were cropped and exported using the Zeiss Zen Black software. The length of the epithelial tongue was measured using Image J. The length of nascent epidermis outgrowing from both wound edges was expressed as a percentage of the total length of the wound bed to get the percentage of re-epithelialization for each sample.

2.16 | Quantification of inflammatory cells in rat wound tissue sections

Two ROIs (250 µm by 250 µm) from H&E-stained sections at the wound edges interfacing with the secretome were cropped and exported using the Zeiss Zen Black software. The number of macrophages and neutrophils were quantified manually with the assistance of the Image J counter tool. Individual inflammatory cells were identified by their nuclear morphology.

2.17 | Quantification of fibroblasts and blood vessels in rat wound tissue sections

Tile scan images of H&E-stained sections were analysed using Zeiss Zen Black software to select three regions of

interest (250 μm by 250 μm for fibroblast and 500 μm by 500 μm for blood vessels) for subsequent quantification of fibroblasts and blood vessels using Image J counter tool.

2.18 | Equipment, reagents, and chemicals

DMEM (#11054020), Glutamax (#35050061), NEAA (#11140050), TrypLE™ (#12563011), PBS (#20012027), PFA (#28906), Trypan Blue (#15250061), and StemPro™ chondrogenesis (#A1007101) /osteogenesis (#A1007201) differentiation kit were from Gibco, Life Technologies, USA. FBS (#SV30160.03HI) and HBSS (#SH30588.01) were from HyClone, Cytiva, USA. Penicillin–streptomycin (#L0022) was from Biowest, France. Cryos-tor10 (#07930) was from Biolife Solutions, USA. MesenCult™ adipogenic differentiation kit (#05412) was from Stem Cell Technologies, Canada. Safranin O (#TMS-009-C), crystal violet (#V5265), Oil Red O (#O1391), Alcian Blue (#TMS-010-C) and Alizarin Red (#TMS-008-C) staining solutions, concentrated hydrochloric acid (#320331), sodium bicarbonate (#S6014), magnesium sulphate (#M7506), Limonene mounting medium (#O8015) and Pluronic (#P2443) were from Sigma Aldrich, USA. Human recombinant monoclonal anti-CD14 (#130–110-518), CD34 (#130–120-514), CD45 (#130–110-771), CD73 (#130–111-909), CD90 (#130–114-859), and CD166 (#130–119-769) were from Miltenyi Biotech, Germany. Mouse monoclonal anti-CD105 (#800506) antibody was from Biolegend, USA. Mouse monoclonal anti-K10 (#M7002) was from Dako (Agilent Technologies, Santa Clara, California, USA). Mouse monoclonal anti-K14 was a gift from E. Birgitte Lane's lab (Skin Research Institute of Singapore, A*STAR). Mouse monoclonal anti-p63 (#Ab735) was from Abcam (AbCam, Cambridge, UK). Human recombinant FGF2 (#130–104-924), EGF (#130–097-749), TGF-beta (#130–095-067), and PDGF-BB (#130–108-163) were from Miltenyi Biotech, Germany.

2.19 | Statistical analyses

Data are expressed as mean \pm standard deviation (S.D) or standard error of the mean (S.E.M). Graphpad Prism 8.0 was used to perform statistical analysis. All data amenable to statistical analysis were subjected to Shapiro–Wilk test to ascertain for normality. Normally distributed data was analysed with parametric statistical tests. Comparison between two groups was performed using Student's independent *t*-test. Multiple comparisons were subjected to one-way analysis of variances (ANOVA) followed by

Tukey's post hoc test to ascertain statistical significance. If data was not normally distributed, non-parametric tests, Kruskal Wallis and Mann Whitney *U*-tests, were used. *p*-values <0.05 were considered statistically significant.

3 | RESULTS

3.1 | Characterisation of human Wharton's jelly stem cells and secretome from high density 2-dimensional (2D) hWJSC culture

In-house derived human Wharton's jelly stem cells (hWJSCs) were successfully isolated and cultured. Flow cytometry, differentiation and assessment of cell phenotype were used to determine if the cells were mesenchymal stem cells. Flow cytometry analysis of the cultured hWJSCs at passage 3 showed that the cells were positive for CD73, CD90, CD105, CD166 and negative for CD14, CD34, CD45 (Figure 1A). The cells were plastic adherent with a fibroblastic morphology and could undergo adipogenesis, osteogenesis and chondrogenesis (Figure 1B). These characteristics satisfy the minimum criteria for mesenchymal stem cells (MSCs)³¹ and the cells were used for secretome production.

The human WJSCs were cultured to a high density (greater than 95% confluency) in Corning® HYPERFlasks® (mimics industrial scale system) prior to initiating secretome production. The secretome produced from this high density hWJSC culture was collected, concentrated, and analysed. Total protein concentration of concentrated secretome was approximately 6000 $\mu\text{g}/\text{mL}$. Extracellular vesicle concentration was approximately 825 $\mu\text{g}/\text{mL}$. Factors in concentrated secretome were analysed using an antibody based multiplex screening panel comprising 48 analytes and the concentrations are shown in Table 1. Of the 48 analytes, granulocyte colony stimulating factor (G-CSF), hepatocyte growth factor (HGF), interleukin 6 (IL6), interleukin 8 (IL8) and stem cell growth factor-beta (SCGFbeta) were present at the highest concentrations (>50 ng/mL). This was followed by growth-related oncogene alpha (GROalpha), leukaemia inhibitory factor (LIF), macrophage chemotactic protein 1 (MCP1) and TNF-related apoptosis inducing ligand (TRAIL) at 20–50 ng/mL. Most analytes³⁰ were below 10 ng/mL.

3.2 | Effect of secretome on cell proliferation and 2D scratch assay closure

HaCaT keratinocytes and human dermal fibroblasts (HDF) were treated with secretome at 0, 30, 100, and

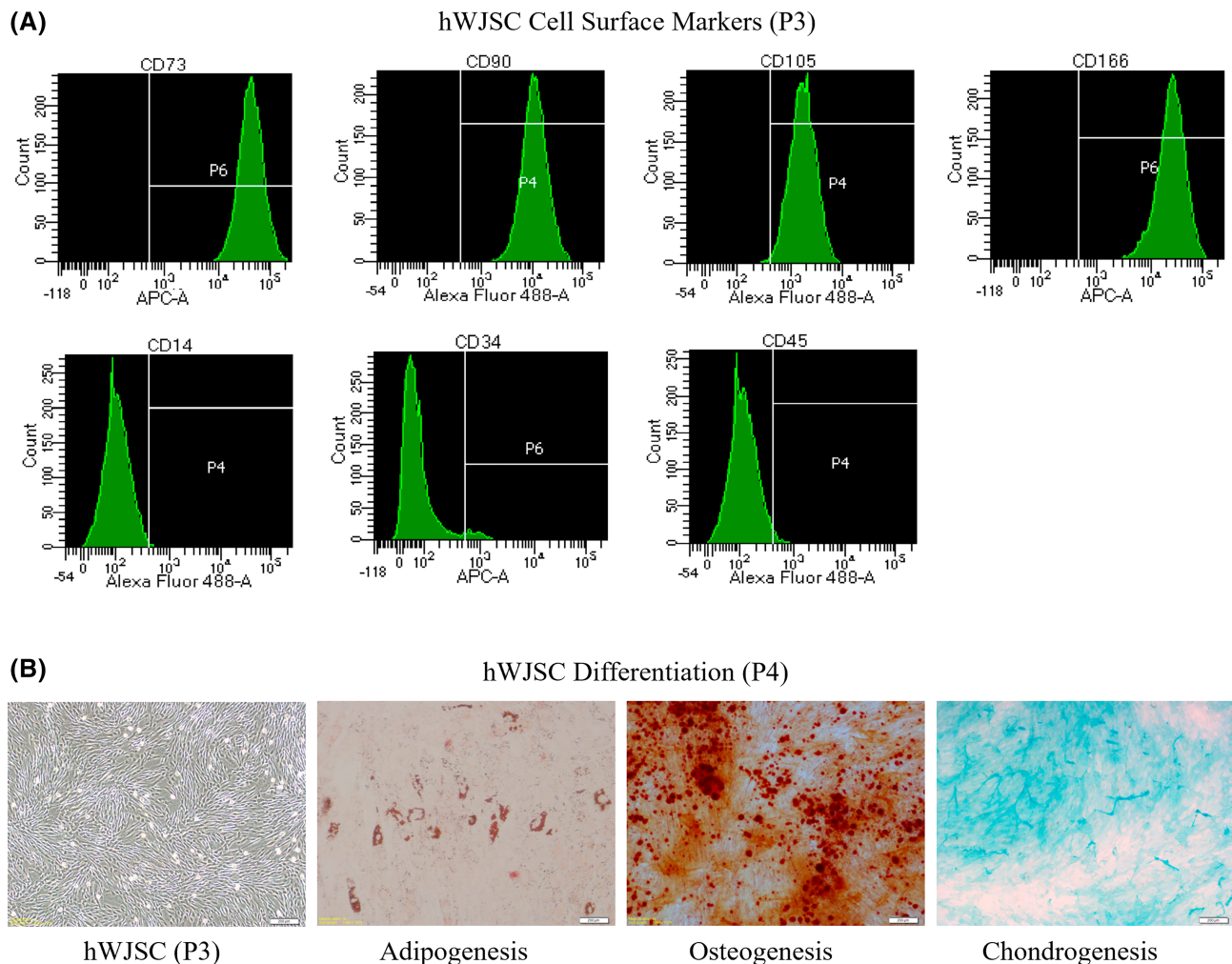


FIGURE 1 Characterisation of hWJSC. (A) Cell surface marker expression of hWJSCs at Passage 3 by flow cytometry. (B) hWJSC morphology (left most image) at Passage 3 and differentiation capacity (right 3 images) of hWJSCs at Passage 4. Orange-brown droplets indicate positive adipogenesis, reddish-brown deposits indicate positive osteogenesis, intense blue extracellular streaks indicate positive chondrogenesis. Scale bar = 200 μ m.

300 μ g/mL for 3 days to assess effects of secretome on cell proliferation. secretome dose-dependently increased both HaCaT and HDF proliferation, with 300 μ g/mL showing the greatest effect (Figure 2A,B). Based on these results, secretome was tested at 300 μ g/mL in a 2D scratch assay to assess its potential in wound healing. HaCaT keratinocytes and human dermal fibroblasts (HDF) were treated with 300 μ g/mL secretome for three (HaCaT keratinocytes) or two (HDF) days after scratching. For both HaCaT and HDF cells, secretome-treated scratches showed an increase in scratch closure compared to those treated with secretome control (Figure 2C,D). Consequently, secretome was tested at 300 μ g/mL based on total protein concentration for both DED-HSE and in vivo wound closure studies.

3.3 | Effect of secretome on DED-HSE wound closure

To assess wound healing effects in a more physiological model, wounded DED-HSEs ($n = 6$) were left untreated or treated with FBS, secretome, and control medium on days 0, 1 and 2 after wound creation. Wound closure was assessed by MTT staining at days 4 and 7 post-wounding. Secretome treatment resulted in significant acceleration of wound closure compared to media control and untreated (blank) wounds (** $p < 0.01$ at day 4 and 7). Secretome-treated wounds were almost fully healed by day 4, similar to the FBS-treated positive controls (p -value = 0.15 at day 4, p -value = 0.52 at day 7, secretome vs. FBS) (Figure 3A,B).

TABLE 1 Concentration of analytes in concentrated secretome.

Analyte	Concentration (ng/mL)	Analyte	Concentration (ng/mL)	Analyte	Concentration (ng/mL)
Basic FGF	3.01	IL-17	0.37	MCP-1 ^a	22.57
B-NGF	0.13	IL-18	0.24	MCP-3	16.80
CTACK	0.68	IL-1a	4.53	M-CSF	0.81
Eotaxin	12.43	IL-1b	0.31	MIF	5.91
G-CSF ^b	522.20	IL-1ra	8.39	MIG	1.26
GM-CSF	0.26	IL-2	0.25	MIP-1a	0.06
GRO-a ^a	39.41	IL-2Ra	1.48	MIP-1b	0.54
HGF ^b	78.69	IL-3	0.03	PDGF-BB	3.84
IFN- α 2	0.46	IL-4	0.25	RANTES	1.17
IFN- γ	4.51	IL-5	4.52	SCF	12.58
IL-10	0.08	IL-6 ^b	137.31	SCGF-b ^b	1399.51
IL-12 (p40)	6.62	IL-7	0.33	SDF-1a	8.45
IL-12 (p70)	0.10	IL-8 ^b	233.11	TNF-a	3.33
IL-13	0.10	IL-9	1.60	TNF-b	0.83
IL-15	8.40	IP-10	0.88	TRAIL ^a	38.59
IL-16	0.53	LIF ^a	22.55	VEGF	0.00

Note: List of factors in screening panel and their respective concentrations in 1 mL of concentrated secretome.

^aConcentration present between 20 and 50 ng/mL.

^bConcentration above 50 ng/mL.

H&E staining of DED-HSE cross sections showed that both secretome and FBS treatments led to faster re-epithelialisation by day 4, with a thicker proliferative epidermal layer seen in secretome-treated wounds (Figure 4A). By day 7, secretome-treated epidermis were fully mature, with a thin proliferative/migratory basal epidermis and thick stratum corneum compared to FBS-treated DED.HSE, which showed mostly proliferative/migratory basal epidermis (Figure 4B). IHC staining with Keratin 14 and P63 confirmed more advanced differentiation of the newly formed epidermis in wounds treated with secretome compared to media control at day 7. Thinner proliferative/migratory basal layer and thicker stratum granulosum was observed in neo-epidermis treated with secretome compared to media control, suggesting that secretome accelerated re-epithelialisation and epidermal maturation (Figure 4B).

3.4 | Effect of secretome on wound healing in a rat acute wound model

Pluronic gel with secretome or control medium was observed to have a slower rate of degradation as compared to the base gel alone. To achieve a similar degradation rate previously established in the laboratory as optimal for testing, the percentage of Pluronic in

secretome and media control gel was titrated (Figure S1). Titration studies showed that both secretome and media control gels had similar degradation rates when formulated in a 20% gel. Consequently, secretome and media control was formulated in 20% Pluronic gel for application onto wounds in rats. Wounds ($n = 3$) were left untreated, treated with Pluronic gel with media control, or treated with Pluronic gel with secretome at 0, 1 and 2 days post-wounding, and wounds were harvested for downstream analysis at 3 and 5 days post-wounding.

To assess the efficacy of the secretome on promoting wound healing, the extent of nascent epidermal growth across the wound bed was measured. Wounds treated with secretome demonstrated faster re-epithelialization in comparison with control wounds. As early as day 3 post-wounding, all the wounds treated with secretome had completely re-epithelialized. In contrast, both untreated and control medium-treated wounds remained open at day 3, with some remaining open even at day 5 (Figure 5A,B). In parallel, the effects of secretome treatment on wound vascularisation was assessed by quantifying the number of blood vessels in the newly formed granulation tissue. There was also an observed increase in blood vessel count in secretome-treated wounds compared to media control-treated and untreated wounds on days 3 and 5 post-wounding (Figure 6B,C).

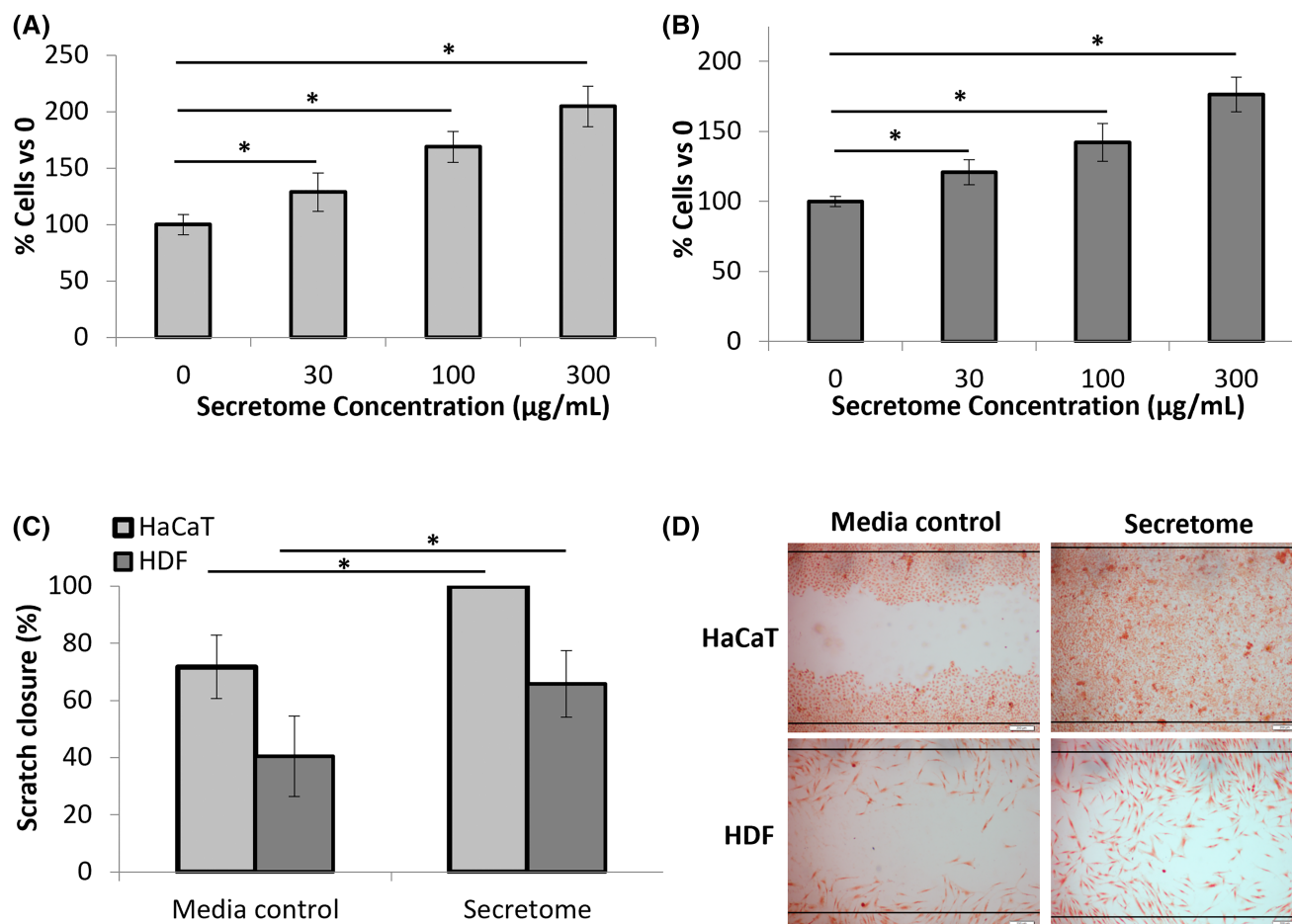


FIGURE 2 (A) Secretome dose response on HaCaT proliferation after 3 days incubation (B) Secretome dose response on HDF proliferation after 3 days incubation (C) Effect of secretome (300 $\mu\text{g/mL}$) on HaCaT and HDF scratch closure after 3 and 2 days incubation, respectively (D) Microscopic images of secretome (300 $\mu\text{g/mL}$) on HaCaT and HDF scratch closure. Black lines indicate initial scratch border. Scale bar = 200 μm . * $p < 0.05$. ($n \geq 12$, 3 experiment sets, where n represents 1 biological repeat).

Neutrophils and macrophages at wound edges interfacing the gel were counted and analysed to investigate the inflammatory reaction under the different treatment conditions. At both day 3 and day 5, secretome-treated wounds had the lowest neutrophil counts among the three groups (Figure 7B,C). Macrophage counts for secretome-treated wounds were the lowest among the three groups at Day 3 (Figure 7B,D). However, on Day 5, an overall increase in macrophage counts were seen for all three groups where secretome-treated groups showed the highest levels of macrophages (Figure 7B,D). Observation of the wound bed suggested that secretome-treated wounds had more mature granulation tissue. To determine if new ECM was being deposited, fibroblast infiltration within the newly formed granulation tissue was quantified. There was a greater degree of fibroblast infiltration in the secretome-treated wounds compared to media control-treated and untreated wounds on both day 3 and 5 post-wounding (Figure 8B,C).

4 | DISCUSSION

In this study, we investigated the potential of secretome derived from prolonged culture of high-density industrial scale 2D human Wharton's jelly stem cells (hWJSCs) in promoting wound healing. Our results reveal evidence of the remarkable efficacy of hWJSC-secretome in accelerating wound closure and enhancing tissue regeneration both in vitro and in vivo.

The accelerated wound closure observed in DED-HSEs treated with secretome corroborates the in vitro proliferation and scratch assay results and further underscores its influence on the fundamental processes of epithelial proliferation and differentiation. It is notable that the re-epithelialisation stimulated by FBS, which is rich in growth factors, mostly comprised a proliferative basal layer without the stratum corneum while secretome promoted epidermal differentiation and cornification. This observation suggests that secretome produced by

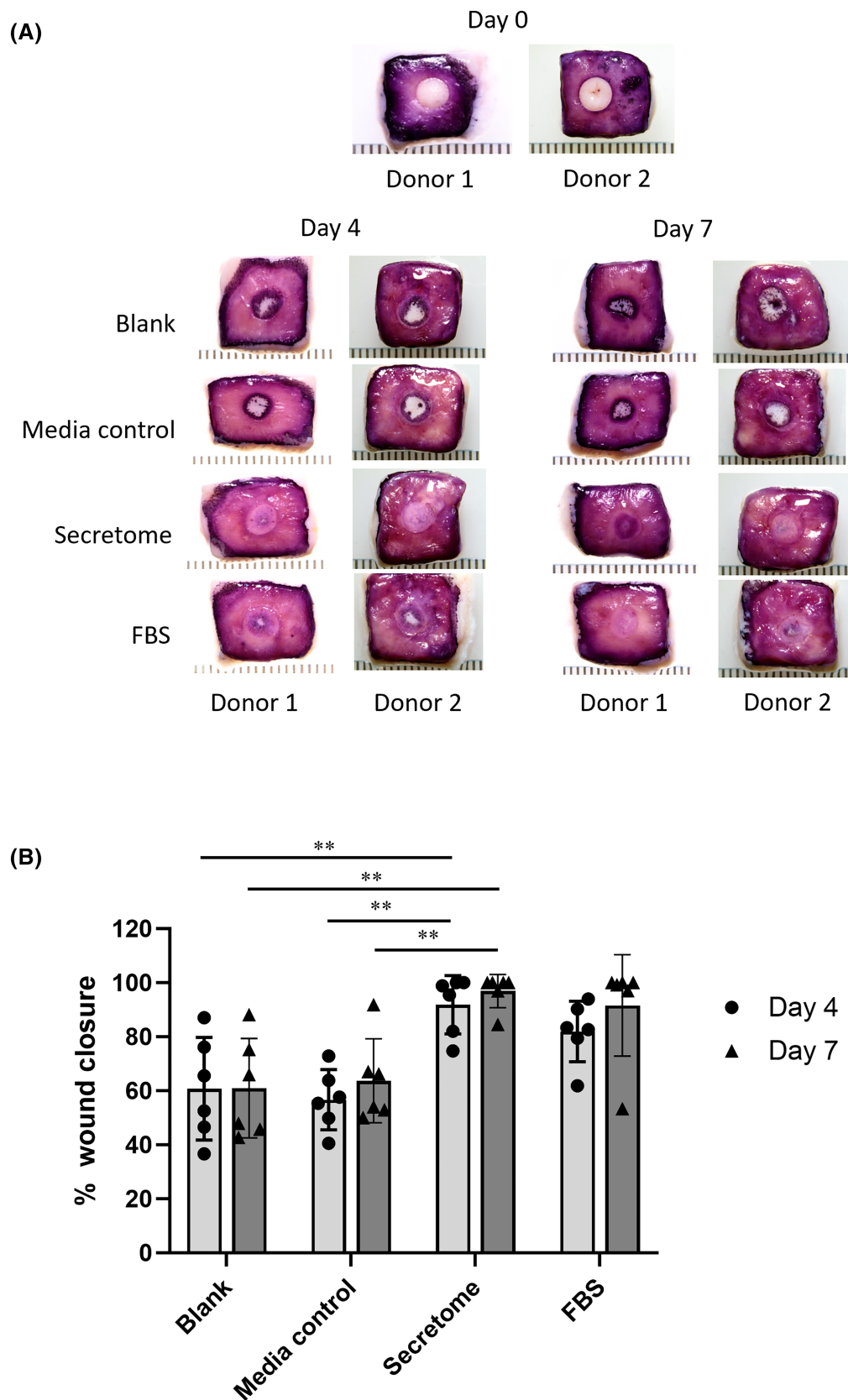


FIGURE 3 DED-HSE re-epithelialisation after wounding and treatment. (A) DED-HSE images after crystal violet staining at Day 0, 4 and 7. Ruler is in mm. (B) Quantification of healed area at Days 4 and 7. $**p < 0.01$. ($n = 6$, where n represents 1 biological repeat).

(A)

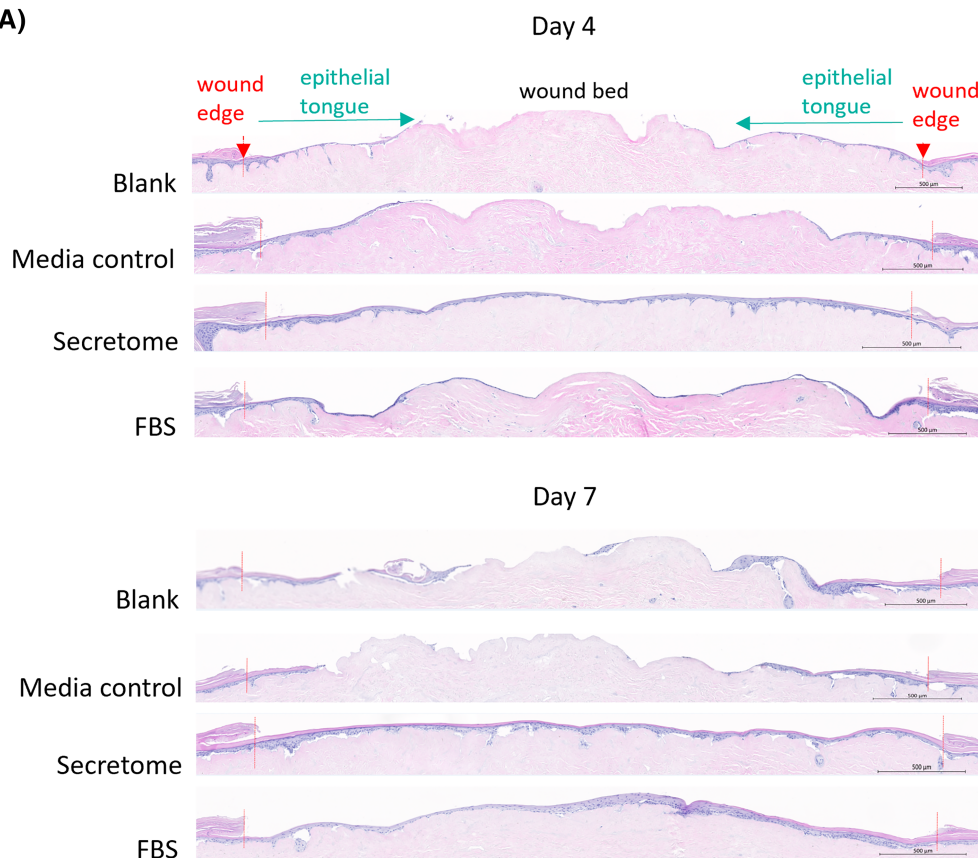
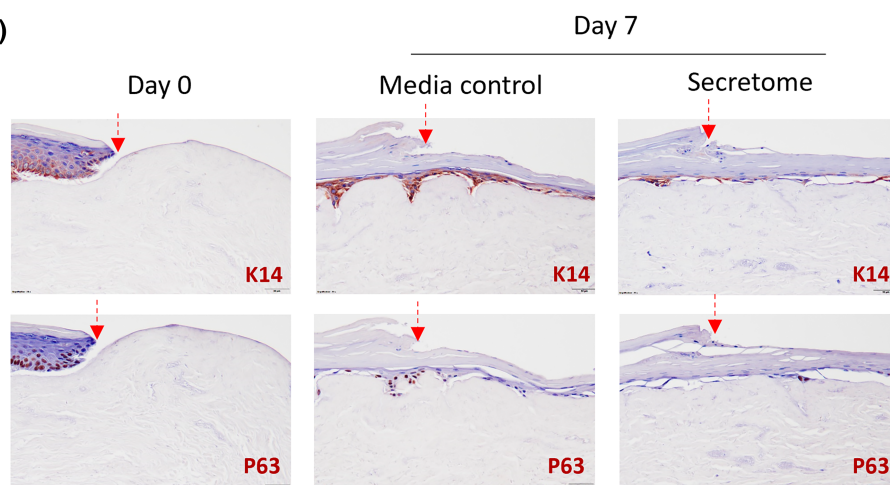


FIGURE 4 DED-HSE cross sections. (A) H&E staining showing re-epithelialisation at Day 4 & 7 post-treatment. Dotted red vertical lines indicate wound edge at day 0. Epithelial tongue (stained purple) can be seen growing inwards from wound edge above wound bed. Scale bar = 500 μm. (B) Keratin 14 (K14) and P63 (both indicative of proliferative epidermis in the basal layer) staining at day 7 after media control or secretome treatment. Scale bar = 30 μm.

(B)



prolonged, high-density industrial scale 2D culture of hWJSCs accelerates epithelial proliferation and its subsequent differentiation into mature skin.

The observed outcomes align with previous studies that highlighted the regenerative potential of stem cell secretome and revealed stimulating factors secreted by WJSCs. Growth factors such as hepatocyte growth factor (HGF) and granulocyte colony stimulating factor

(G-CSF), cytokines such as interleukins 6 and 8 (IL6 and IL8), and extracellular vesicles such as exosomes were detected the hWJSC secretome.^{8,32,33} Importantly, these factors were also present at significant levels in the secretome produced by prolonged 2D culture of hWJSCs at high density.

In the rat acute wound model, the secretome significantly enhanced cutaneous wound healing as evidenced

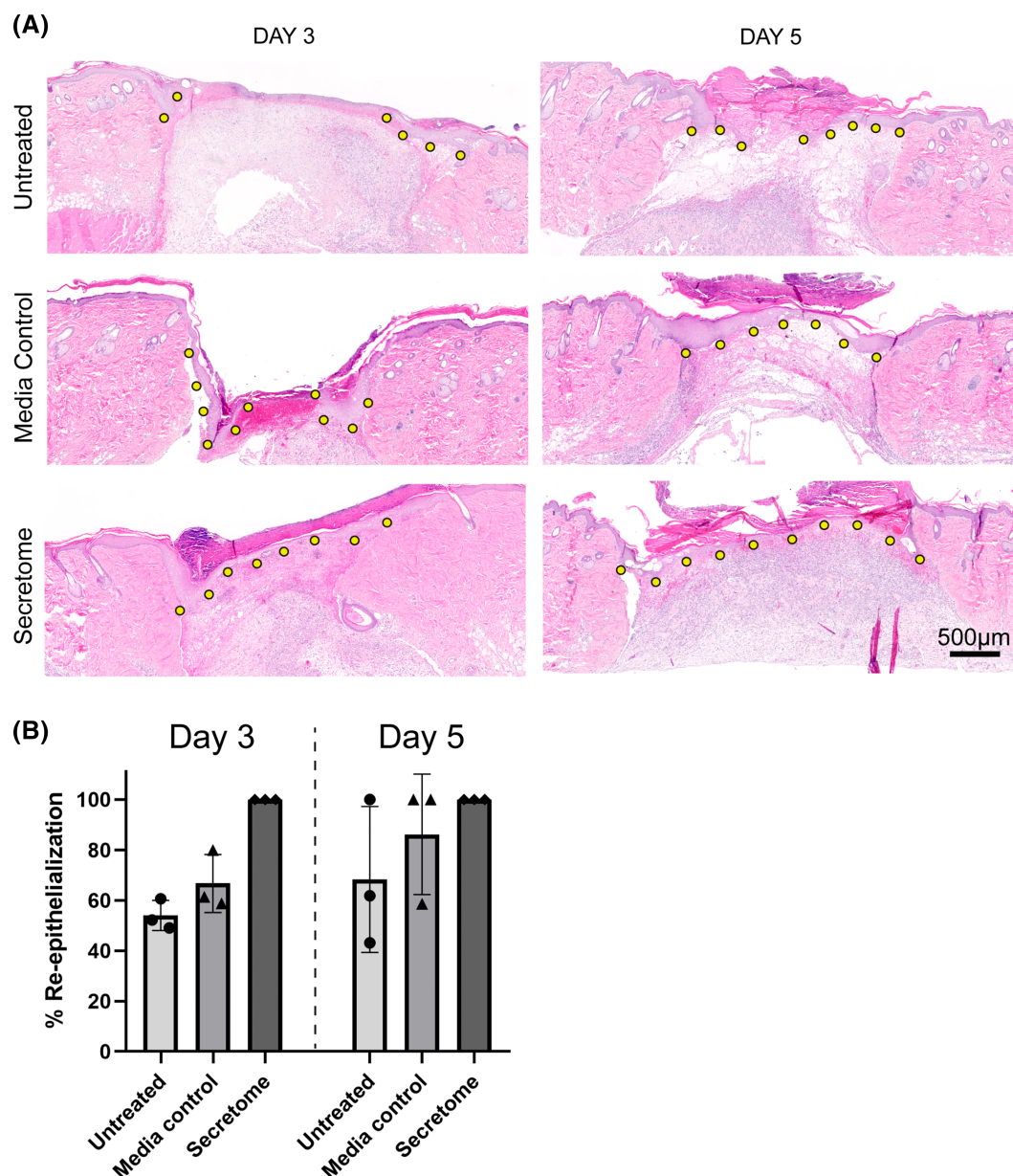


FIGURE 5 Histological analysis of extent of re-epithelialization. (A) Representative H&E images of untreated, media control and untreated wounds on Day 3 and Day 5. Yellow dots outline the length of the nascent epidermis. (B) Quantification of the extent of re-epithelialization on Day 3 and Day 5. ($n \geq 3$, where n represents 1 biological repeat).

by faster wound closure and vascularisation rates, faster resolution of inflammation and increased presence of fibroblast and blood vessels in the newly formed granulation tissue. This has also been observed by others, where conditioned medium from Wharton's jelly stem cells strongly promoted wound healing in rodents.^{22,34,35} Notably, the promotion of re-epithelialisation suggests a direct impact on the restoration of the skin barrier function, which requires epidermis regeneration involving keratinocyte proliferation, differentiation, and migration. This process is also crucial for the prevention of water loss and infection.

Examination of the inflammation at the wound periphery is crucial for understanding the host response to the secretome. During normal healing, neutrophil numbers initially surge in the early inflammatory response, followed by a subsequent decline coinciding with macrophage infiltration to the wound site. The low levels of neutrophil numbers in secretome-treated wounds on both days 3 and 5 suggest that the secretome did not provoke an undesired inflammatory response and possibly resolved inflammation faster. This may explain the rise in macrophage numbers seen in secretome-treated wounds on day 5, which may be attributed to a

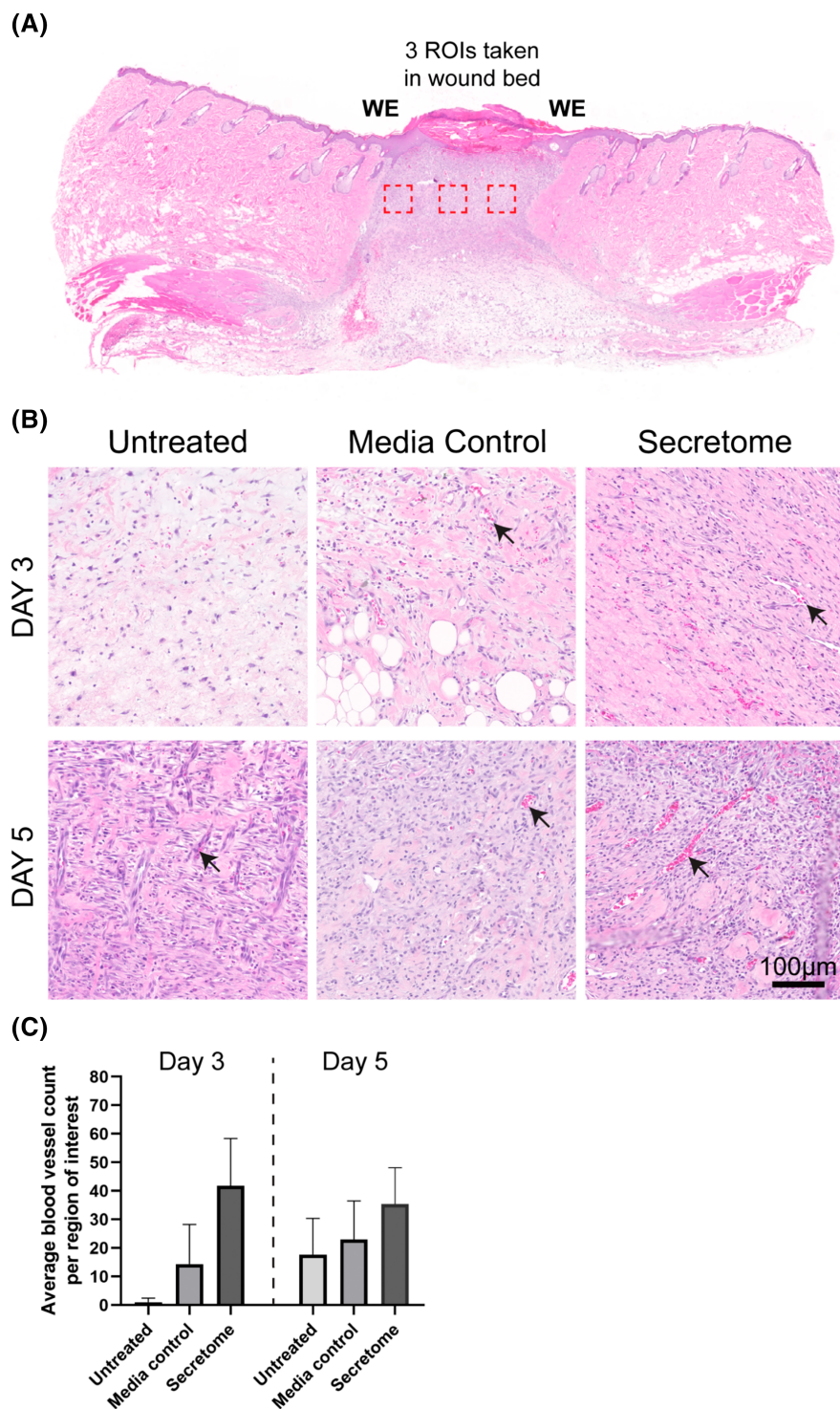


FIGURE 6 Analysis of blood vessel count. (A) Schematic illustrating regions of interest in red boxes. WE, wound edge. Black arrows represent blood vessels. (B) Representative images taken from within wound bed. (C) Quantification of blood vessel count on Day 3 and Day 5. ($n \geq 3$, where n represents 1 biological repeat).

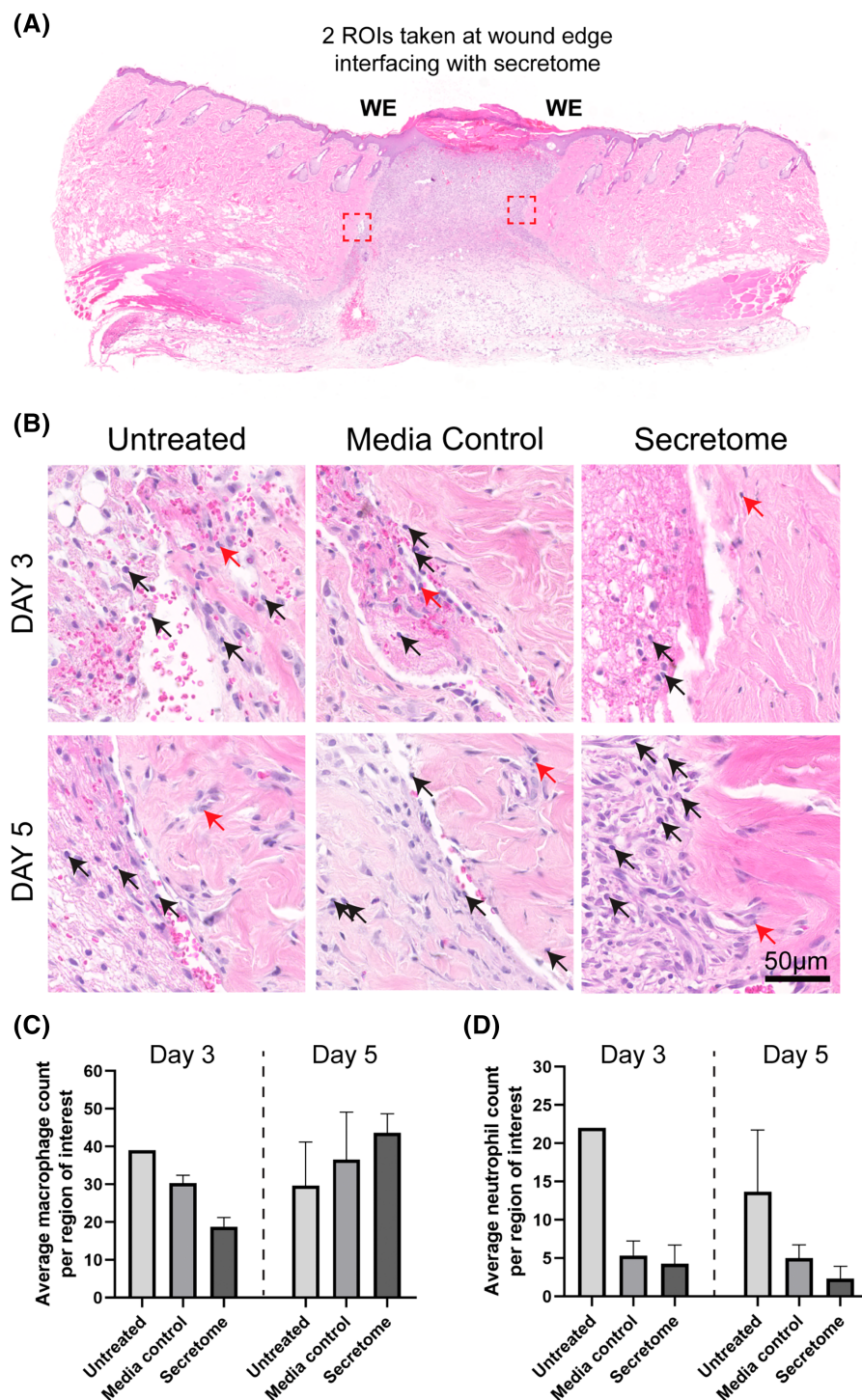
possible increase in M2 macrophages that are crucial for cell proliferation and tissue repair. The immunomodulatory effects of umbilical cord-derived mesenchymal stem cell secretome in wound healing are well documented and have been extensively reviewed.^{18,36}

Presence and activity of fibroblasts in granulation tissue are essential for efficient wound healing and tissue repair as they are responsible for synthesising and

depositing extracellular matrix components that provide structural support and integrity to the healing wound. As the secretome promotes both epithelial and fibroblast proliferation and migration, it corresponds to the observed increased presence of fibroblasts in the wound bed of secretome-treated wounds, which explains the faster re-epithelialization seen in these wounds. Fibroblasts deposit extracellular matrix components, creating a

FIGURE 7 Inflammatory analysis.

(A) Schematic illustrating regions of interest in red boxes. WE, wound edge. Black arrows represent macrophage and red arrows represent neutrophils. (B) Representative images of wound edge interfacing with secretome. (C) Quantification of macrophage count on Day 3 and Day 5. (D) Quantification of neutrophil count on Day 3 and Day 5. ($n \geq 3$, where n represents 1 biological repeat).



scaffold that provides mechanical support and guidance for migrating epithelial cells during re-epithelialization that facilitates wound closure. In addition, fibroblasts also secrete growth factors and cytokines that promote epithelial cell proliferation, differentiation, and migration, which further enhances the secretome effects. In fact, Hendrawan's group showed that human umbilical cord mesenchymal stem cell conditioned medium could promote fibroblast collagen synthesis,³⁷ which supports

our observation of more mature granulation tissue in the wound bed of secretome-treated wounds.

Adequate oxygen and nutrient supply delivered by blood vessels are essential to maintain activity of fibroblasts, keratinocytes, and immune cells that are needed for tissue repair. The enhanced vascularization observed in secretome-treated wounds strongly suggests that the secretome possesses potent pro-angiogenic properties, which facilitates creation of a microenvironment

(A)

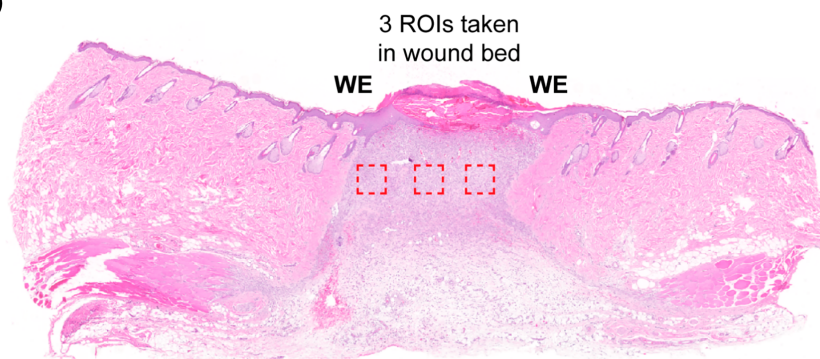
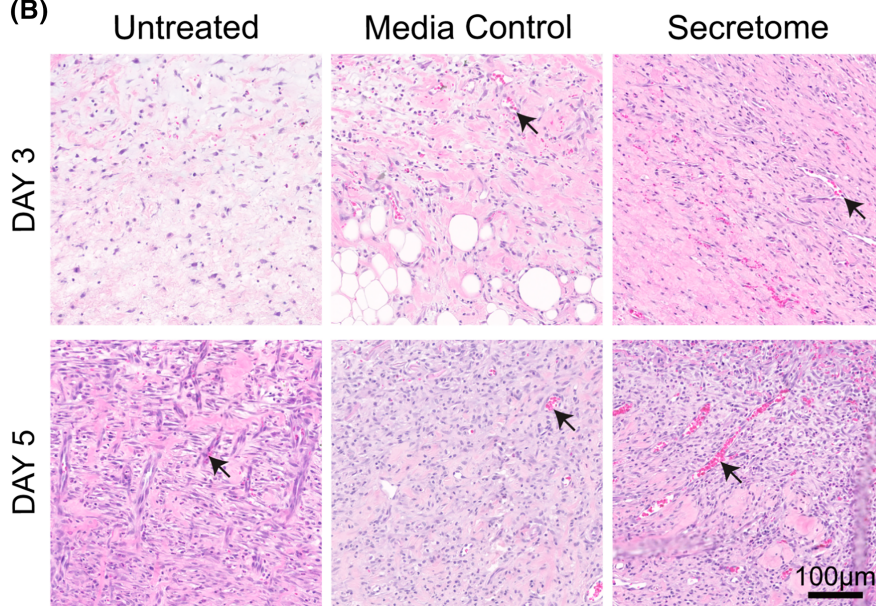
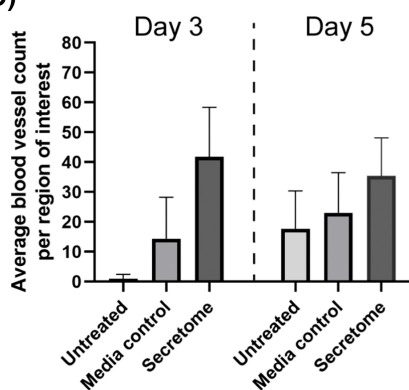


FIGURE 8 Analysis of fibroblast count. (A) Schematic illustrating regions of interest in red boxes. WE, wound edge. Black arrows represent fibroblasts. (B) Representative images taken from within wound bed. (C) Quantification of fibroblast count on Day 3 and Day 5. ($n \geq 3$, where n represents 1 biological repeat).

(B)



(C)



conductive to efficient tissue repair and is consistent with the literature.^{38,39} Taken together, the above study data clearly demonstrates that the secretome has profound effects on multiple facets of wound healing that supports the use of the secretome as a wound therapeutic.

In conclusion, our study demonstrates that the secretome derived from prolonged high-density industrial scale 2D hWJSC culture possesses potent wound healing properties. Therefore, our study indicates that it is

possible to harvest a much larger quantity of factors from a single batch of cells via multiple collections over a prolonged period compared to a single collection. This is crucial in lowering the overall cost of production as the cells explanted from umbilical cords are a high value material and the culture medium and single-use consumables used in expanding the cells are often the most expensive components in the system. The observed enhancements in wound closure, epithelial proliferation, inflammation

resolution, vascularization and granulation maturation hold promising implications for the development of cost-effective and efficacious secretome-based wound healing products.

ACKNOWLEDGEMENTS

The authors thank the Asian Skin Biobank (ASB) at the Skin Research Institute of Singapore (SRIS), especially Alimat A., Lee J., and Yap A., for generating and providing primary epidermal keratinocytes derived from a healthy middle-aged Chinese Female, as well as Assoc Prof Tan BK. from the Department of Plastic, Reconstructive and Aesthetic Surgery, and Dr Chua A. from Singapore General Hospital, Prof Chan Jerry KY. from KK Women's and Children's Hospital, and the SingHealth Tissues Repository's team for providing waste surgical skin tissues to the ASB to develop in vitro skin models (IRB 2020-209). The authors also thank Dr Leavesley D. for his guidance on the DED-HSE model. The development of the DED-HSE platform was funded by Singapore's Agency for Science, Technology & Research (A*STAR) under the Industry Alignment Fund Pre-Positioning Fund (IAF-PP HBMS) H1701a0004 and H1701a00B9. We thank Leigh Madden for his assistance with the animal work. The authors thank Tow Yung Clinic for assisting in donor recruitment and both Tow Yung Clinic and Thomson Medical for collecting umbilical cord waste tissue on behalf of Celligenics Pte Ltd. The authors also thank the Agency for Science, Technology and Research (A*STAR)'s Singapore Immunology Network (SiGN) Multiplex Analysis of Proteins (MAP) platform for enabling the Luminex work for this publication. A*STAR's SiGN MAP platform is supported by research grants including the Biomedical Research Council (BMRC) grant and the National Research Foundation (NRF), Immunomonitoring Service Platform (Ref: ISP: NRF2017_SISFP09) grant.

FUNDING INFORMATION

This research was supported by the Skin Innovation Grant SIG2005 in partnership with Celligenics Pte Ltd.

CONFLICT OF INTEREST STATEMENT

P.M., A.Y., Y.A., are employees of Celligenics Pte Ltd.

DATA AVAILABILITY STATEMENT

The data that support the findings of this study are available from the corresponding author upon reasonable request.

ORCID

Pamela Mok  <https://orcid.org/0009-0008-1940-233X>

REFERENCES

- Guo S, DiPietro LA. Factors affecting wound healing. *J Dent Res.* 2010;89(3):219-229.
- Reinke JM, Sorg H. Wound repair and regeneration. *Eur Surg Res.* 2012;49(1):35-43.
- Järbrink K, Ni G, Sönnnergren H, et al. Prevalence and incidence of chronic wounds and related complications: a protocol for a systematic review. *Syst Rev.* 2016;5(1):152.
- Nussbaum SR, Carter MJ, Fife CE, et al. An economic evaluation of the impact, cost, and Medicare policy implications of chronic nonhealing wounds. *Value Health.* 2018;21(1):27-32.
- Sen CK. Human wounds and its burden: an updated compendium of estimates. *Adv Wound Care (New Rochelle).* 2019;8(2):39-48.
- Ebrahim N, Dessouky AA, Mostafa O, et al. Adipose mesenchymal stem cells combined with platelet-rich plasma accelerate diabetic wound healing by modulating the notch pathway. *Stem Cell Res Ther.* 2021;12(1):392.
- Gao S, Chen T, Wang Z, et al. Immuno-activated mesenchymal stem cell living electrospun nanofibers for promoting diabetic wound repair. *J Nanobiotechnol.* 2022;20(1):294.
- Jiao Y, Chen X, Niu Y, et al. Wharton's jelly mesenchymal stem cells embedded in PF-127 hydrogel plus sodium ascorbyl phosphate combination promote diabetic wound healing in type 2 diabetic rat. *Stem Cell Res Ther.* 2021;12(1):559.
- Zhang J, Qu X, Li J, et al. Tissue sheet engineered using human umbilical cord-derived mesenchymal stem cells improves diabetic wound healing. *Int J Mol Sci.* 2022;23(20):12697.
- Shi Y, Wang S, Zhang W, et al. Bone marrow mesenchymal stem cells facilitate diabetic wound healing through the restoration of epidermal cell autophagy via the HIF-1 α /TGF- β 1/SMAD pathway. *Stem Cell Res Ther.* 2022;13(1):314.
- Abd-Allah SH, El-Shal AS, Shalaby SM, Abd-Elbary E, Mazen NF, Abdel Kader RR. The role of placenta-derived mesenchymal stem cells in healing of induced full-thickness skin wound in a mouse model. *IUBMB Life.* 2015;67(9):701-709.
- Ma H, Siu WS, Leung PC. The potential of MSC-based cell-free therapy in wound healing—a thorough literature review. *Int J Mol Sci.* 2023;24(11):9356.
- Malhotra P, Shukla M, Meena P, et al. Mesenchymal stem cells are prospective novel off-the-shelf wound management tools. *Drug Deliv Transl Res.* 2022;12(1):79-104.
- Liu H, Yang R, Zhao S, et al. Collagen scaffolds derived from bovine skin loaded with MSC-optimized M1 macrophages remodeling and chronic diabetic wounds healing. *Bioeng Transl Med.* 2023;8(3):e10467.
- Hu M, Li Z, Liu Y, et al. Multifunctional hydrogel of recombinant humanized collagen loaded with MSCs and MnO₂ accelerates chronic diabetic wound healing. *ACS Biomater Sci Eng.* 2024;10(5):3188-3202.
- Park KS, Bandeira E, Shelke GV, Lässer C, Lötvall J. Enhancement of therapeutic potential of mesenchymal stem cell-derived extracellular vesicles. *Stem Cell Res Ther.* 2019;10(1):288.
- Vizoso F, Eiro N, Cid S, Schneider J, Perez-Fernandez R. Mesenchymal stem cell Secretome: toward cell-free therapeutic strategies in regenerative medicine. *Int J Mol Sci.* 2017;18(9):1852.

18. Montero-Vilchez T, Sierra-Sánchez Á, Sanchez-Diaz M, et al. Mesenchymal stromal cell-conditioned medium for skin diseases: a systematic review. *Front Cell Dev Biol.* 2021;9:654210.
19. Zhang Y, Bai X, Shen K, et al. Exosomes derived from adipose mesenchymal stem cells promote diabetic chronic wound healing through SIRT3/SOD2. *Cells.* 2022;11(16):2568.
20. Yang J, Chen Z, Pan D, Li H, Shen J. <p>umbilical cord-derived mesenchymal stem cell-derived exosomes combined Pluronic F127 hydrogel promote chronic diabetic wound healing and complete skin regeneration</p>. *Int J Nanomedicine.* 2020;15:5911-5926.
21. Rezaie J, Feghhi M, Etemadi T. A review on exosomes application in clinical trials: perspective, questions, and challenges. *Cell Commun Signal.* 2022;20(1):145.
22. Fong C, Tam K, Cheyyatraivendran S, et al. Human Wharton's jelly stem cells and its conditioned medium enhance healing of excisional and diabetic wounds. *J Cell Biochem.* 2014;115(2):290-302.
23. Ormazabal V, Nova-Lampeti E, Rojas D, et al. Secretome from human mesenchymal stem cells-derived endothelial cells promotes wound healing in a Type-2 diabetes mouse model. *Int J Mol Sci.* 2022;23(2):941.
24. Sun J, Zhang Y, Song X, Zhu J, Zhu Q. The healing effects of conditioned medium derived from mesenchymal stem cells on radiation-induced skin wounds in rats. *Cell Transplant.* 2019;28(1):105-115.
25. Chen S, bin Abdul Rahim AA, Mok P, Liu D. An effective device to enable consistent scratches for in vitro scratch assays. *BMC Biotechnol.* 2023;23(1):32.
26. Schindelin J, Arganda-Carreras I, Frise E, et al. Fiji: an open-source platform for biological-image analysis. *Nat Methods.* 2012;9(7):676-682.
27. Xie Y, Rizzi SC, Dawson R, et al. Development of a three-dimensional human skin equivalent wound model for investigating novel wound healing therapies. *Tissue Eng Part C Methods.* 2010;16(5):1111-1123.
28. Bancroft JD, Gamble M. In: Bancroft JD, Gamble M, eds. *Theory and Practice of Histological Techniques*. 5th ed. Churchill Livingstone; 2002.
29. Taylor CR, Shi SR, Chen C, Young L, Yang C, Cote RJ. Comparative study of antigen retrieval heating methods: microwave, microwave and pressure cooker, autoclave, and steamer. *Biotech Histochem.* 1996;71(5):263-270.
30. Shi SR, Key ME, Kalra KL. Antigen retrieval in formalin-fixed, paraffin-embedded tissues: an enhancement method for immunohistochemical staining based on microwave oven heating of tissue sections. *J Histochem Cytochem.* 1991;39(6):741-748.
31. Dominici M, Le Blanc K, Mueller I, et al. Minimal criteria for defining multipotent mesenchymal stromal cells. The International Society for Cellular Therapy position statement. *Cytotherapy.* 2006;8(4):315-317.
32. Maurya DK, Bandekar M, Sandur SK. Soluble factors secreted by human Wharton's jelly mesenchymal stromal/stem cells exhibit therapeutic radioprotection: a mechanistic study with integrating network biology. *World J Stem Cells.* 2022;14(5):347-361.
33. Song J y, Kang HJ, Ju HM, et al. Umbilical cord-derived mesenchymal stem cell extracts ameliorate atopic dermatitis in mice by reducing the T cell responses. *Sci Rep.* 2019;9(1):6623.
34. Mathen C, Ghag Sawant M, Gupta R, Dsouza W, Krishna SG. Evaluation of potential application of Wharton's jelly-derived human mesenchymal stromal cells and its conditioned Media for Dermal Regeneration using rat wound healing model. *Cells Tissues Organs.* 2021;210(1):31-44.
35. Arno AI, Amini-Nik S, Blit PH, et al. Human Wharton's jelly mesenchymal stem cells promote skin wound healing through paracrine signaling. *Stem Cell Res Ther.* 2014;5(1):28.
36. Li X, Zhang D, Yu Y, Wang L, Zhao M. Umbilical cord-derived mesenchymal stem cell secretome promotes skin regeneration and rejuvenation: from mechanism to therapeutics. *Cell Prolif.* 2024;57(4):e13586.
37. Hendrawan S, Kusnadi Y, Lagonda CA, et al. Wound healing potential of human umbilical cord mesenchymal stem cell conditioned medium: an in vitro and in vivo study in diabetes-induced rats. *Vet World.* 2021;14:2109-2117.
38. Shen C, Lie P, Miao T, et al. Conditioned medium from umbilical cord mesenchymal stem cells induces migration and angiogenesis. *Mol Med Rep.* 2015;12(1):20-30.
39. Huynh PD, Van Pham P, Vu NB. Exosomes derived from human umbilical cord mesenchymal stem cells enhance angiogenesis through upregulation of the VWF and Flk1 genes in endothelial cells. *Adv Exp Med Biol.* 2023. doi:10.1007/5584_2023_768

SUPPORTING INFORMATION

Additional supporting information can be found online in the Supporting Information section at the end of this article.

How to cite this article: Chin JS, Tan MLL, Lim PLK, et al. Secretome from prolonged high-density human Wharton's jelly stem cell culture accelerates wound healing in both in vitro and in vivo models. *Int Wound J.* 2025;22(5):e70033. doi:10.1111/iwj.70033